Optica Applicata, Vol. XXXVII, No. 4, 2007

Resonant microcavity enhanced infrared photodetectors

JANUSZ KANIEWSKI[1], JAN MUSZALSKI[1], JÓZEF PIOTROWSKI[2]

[1]Institute of Electron Technology, al. Lotników 32/46, 02-668 Warsaw, Poland

[2]Vigo System S.A., ul. Świetlików 3, 01-493 Warsaw, Poland

Resonant cavity enhanced (RCE) infrared photodetectors are used in many applications due to their high quantum efficiency and large bandwidth. Therefore, wide device diversity is desired. In this paper, recent tendencies in design and fabrication of these devices are presented. Various issues for InGaAs/InAlAs/InP RCE detectors operating at 1.55 μm and HgCdTe/CdTe/GaAs RCE devices dedicated for 10.6 μm radiation detection are discussed. The detector structures were grown by means of two industry standard technologies, *i.e.*, molecular beam epitaxy and metaloorganic chemical vapor deposition. Optimized devices can be optically integrated with monolithic microlenses.

Keywords: optoelectronic device characterization, design, and modeling; III–V and II–VI semiconductors.

1. Introduction

High-speed and high-efficiency infrared detectors play an important role in optical communication and measurement systems. The efficiency of conventional detectors has been limited, mostly due to the thin absorption region needed for short transit times. One can increase the absorber thickness to achieve higher efficiencies, but this also means longer transit times which will degrade the high-speed performance of the devices. Resonant cavity enhanced photodetectors (RCE PDs) potentially offer the possibility of overcoming this limitation of the bandwidth-efficiency product of conventional photodetectors [1–3]. The RCE devices are based on the enhancement of the optical field within the Fabry–Perot resonant cavity. The increased field allows the usage of thin absorbing layers, which minimizes the transit time of the photo-carriers without hampering the quantum efficiency. High speed RCE photodetector research has mainly concentrated on using p-i-n photodiodes. In this paper, different strategies in utilizing resonant cavity properties in improving the performance of p-i-n detectors are considered.

2. Device design

The optical design of the photodiodes was accomplished using transfer matrix method (TMM) based theoretical simulations. Spectral reflectivity and responsivity simulations were carried out to find the desired epitaxial structure. The devices were optimized for backside illumination through the substrate. We have considered two different material systems for very different spectral bands: InGaAs/InAlAs/InP and HgCdTe/CdTe/GaAs for operation at 1.55 μm and 10.6 μm wavelength, respectively. The surfaces of all the detectors were covered with antireflective coatings.

2.1. $In_xGa_{1-x}As/In_xAl_{1-x}As/InP$ RCE photodiodes

The InGaAs/InAlAs/InP RCE PD structure was optimized for small angle operation to detect near normal 1.55 μm incident radiation. A diagram showing the cross-section of the simulated device is presented in Fig. 1.

Au		
DBR 9x	Si_3N_4	259.2 nm
	SiO_2	205.4 nm
Contact	InAlAs:Be $p = 1\cdot10^{19}$ cm^{-3}	162.9 nm
	InAlAs:Be $p = 2\cdot10^{18}$ cm^{-3}	300.0 nm
	InAlAs undoped	30.0 nm
Absorber	InGaAs undoped	140.0 nm
	InAlAs undoped	30.0 nm
	InAlAs:Si $n = 3\cdot10^{18}$ cm^{-3}	253.1 nm
Contact DBR 7x	InGaAs:Si $n = 1\cdot10^{19}$ cm^{-3}	108 nm
	InAlAs:Si $n = 1\cdot10^{19}$ cm^{-3}	120.4 nm
Buffer	InAlAs:Si $n = 3\cdot10^{18}$ cm^{-3}	2 287.4 nm
Substrate	InP:Fe	350 000.0 nm

Fig. 1. Design of the InGaAs/InAlAs /InP RCE p-i-n PD.

The device heterostructure consists of a 2287.4 nm thick Si doped $In_{0.52}Al_{0.48}As$ buffer layer deposited directly on InP substrate. This layer is followed by DBR which is made of 7 pairs of quarter wavelength $(In_{0.52}Al_{0.48}As/In_{0.53}Ga_{0.47}As)$:Si layers designed for high reflectance of 1.55 μm radiation. Carrier concentration in DBR layers is equal to 10^{19} cm^{-3}. It results in the shift of the absorption edge of the $In_{0.53}Ga_{0.47}As$ layers beyond the spectral range of interest. This shift is caused by Burstein's effect associated with conduction band filling with carriers. The 140 nm thick $In_{0.53}Ga_{0.47}As$ undoped absorbing layer is placed in a $5\lambda/2$ cavity, between two $In_{0.52}Al_{0.48}As$ spacer layers of total thickness 283.1 nm and 492.9 nm, respectively. They consists of several undoped and doped thinner layers. Contact layers are depicted in Fig. 1. After epitaxial growth on the top surface of heterostructures hybrid mirrors consisting of dielectric Si_3N_4/SiO_2 DBR and Au layers were deposited.

2.2. $Hg_xCd_{1-x}Te$/CdTe/GaAs RCE photodiodes

Optical resonance enhancement was successfully used for photoconductors, photoelectromagnetic and short wavelength photodiodes, see [4–6] and original paper cited therein. The present efforts are concentrated on long (≈ 10 µm) wavelength photodiodes optimized for fast and sensitive detection of quantum cascade laser radiation. The long wavelength photodiodes operating without cryocooling are characterized by large dark currents and low resistances due to huge thermal generation of charge carriers [4]. The total thermal generation has been minimized by reduction of absorber volume. An efficient way is the use of optical concentrators, such as immersion lenses that make it possible to decrease the physical area of the detectors by a large factor compared to their optical area [4]. For example, the area gain of ≈ 120 is being achieved with GaAs hemispherical lenses [6]. Further reduction of the thermal dark current could be obtained by reduction of absorber thickness below normal absorption depths and use of the optical resonance to prevent loss of quantum efficiency. The design of optically immersed $Hg_xCd_{1-x}Te$/CdTe/GaAs RCE photodiodes is a more complex task since the devices must be optimized to operate within a wide range of incidence angles. Several approaches to cope with the problem have been tried. An example is the device with the structure shown in Fig. 2. The device structures were grown on the CdTe buffer layer deposited directly on GaAs substrate. Detector N^+-p-P^+ structure was placed between the front and back DBRs. Three types of structures differing in the number of layer pairs forming the front DBR

Au		
DBR 3x	CdTe	985.7 nm
	HgCdTe, x = 0.35	821.0 nm
Contact	HgCdTe, x = 0.35; P^+	**Type 1 – DBR 7x** – 3 910.9 nm **Type 2 – DBR 3x** – 2 975.5 nm **Type 3 – DBR 0x** – 1 856.0 nm
Absorber	HgCdTe, x = 0.185; p	**Type 1 – DBR 7x** – 310.0 nm **Type 2 – DBR 3x** – 2 072.2 nm **Type 3 – DBR 0x** – 4 000.4 nm
Contact	HgCdTe, x = 0.35; N^+	**Type 1 – DBR 7x** – 6 373.9 nm **Type 2 – DBR 3x** – 5 438.5 nm **Type 3 – DBR 0x** – 4 319.0 nm
Type 1 – DBR 7x **Type 2 – DBR 3x** **Type 3 – DBR 0x**	CdTe	985.7 nm
	HgCdTe, x = 0.35	821.0 nm
Buffer	CdTe	4 928.4 nm
Substrate	GaAs:Si	400 000.0 nm

Fig. 2. Schematic structure of HgCdTe/CdTe/GaAs RCE N^+-p-P^+ photodiode.

were studied. They consisted of 7, 3 or 0 pairs of HgCdTe, $x = 0.35$ and CdTe layers and were optimized for 10.6 μm wavelength reflection. The changes of pair number result in changes of DBR reflection. To ensure 92% absorption, modification of absorber thickness was needed. In optimized RCE devices the thickness of N^+ and P^+ HgCdTe, $x = 0.35$ layers placed just at the absorber layer had to be modified as well.

The thicknesses of the layers for three types of the structures studied are depicted in Fig. 2. On the top of the structures a second reflector was placed. In all the structures it consisted of 3 DBRs, formed by HgCdTe and CdTe layers, and Au layer. Reflection of the top mirror was over 98% in all the structures studied.

3. Experimental details

The InGaAs/InAlAs/InP RCE PD structures were grown by molecular beam epitaxy (MBE) using Riber 32P system. Lattice matched epitaxial layers of $In_{0.53}Ga_{0.47}As$ and $In_{0.52}Al_{0.48}As$ were grown on (001) oriented InP substrates. The composition of the layer was determined from X-ray diffraction studies using MRD-PHILIPS diffractometer in the double and triple axis configurations. Carrier concentrations were determined from the Hall effect studies performed on test layers. The dielectric layers were deposited in plasma enhanced chemical vapor deposition (PECVD) process.

The HgCdTe/CdTe/GaAs RCE PD structures were grown by metaloorganic chemical vapor deposition using Aixtron 200 system. Thick (0.5–3 mm) semi-insulaing GaAs substrates were used to make fabrication of the device compatible with the monolithic optical immersion technology in which microlenses were formed directly in epitaxial layer [7].

4. Results and discussion

Back reflectors in the InGaAs/InAlAs/InP RCE PDs are often made of InGaAs and InAlAs layers. One disadvantage of this system is the poor refractive index contrast between both materials. Roughly, 35 periods are required for a near unity reflectivity mirror. In the detector structure proposed in this paper semiconductor DBR was replaced by hybrid reflector – SiO_2/Si_3N_4+Au. Using 9 pairs of SiO_2/Si_3N_4 high total reflection of 1.55 μm radiation of hybrid reflector $R_2 = 0.995$ was achieved. Low reflective front reflector consisted of 7 pairs of InGaAs and InAlAs layers only and it was made in the MBE process. Numerically simulated distribution of electromagnetic field across InGaAs/InAlAs/InP is presented in Fig. 3. Undoped InGaAs absorption layer is placed in maximum field intensity to allow efficient radiation absorption. Spectral photoresponse of the fabricated p-i-n photodiodes is presented in Fig. 4. In simulated spectra small oscillations related to parasitic Fabry–Perot modes have

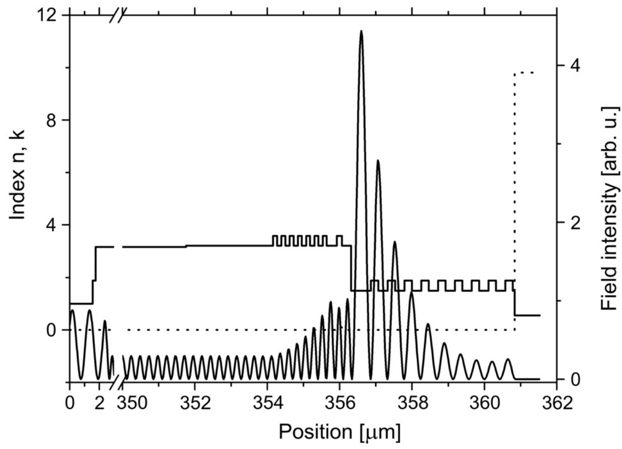

Fig. 3. Distribution of field intensity across InGaAs/InAlAs/InP structure.

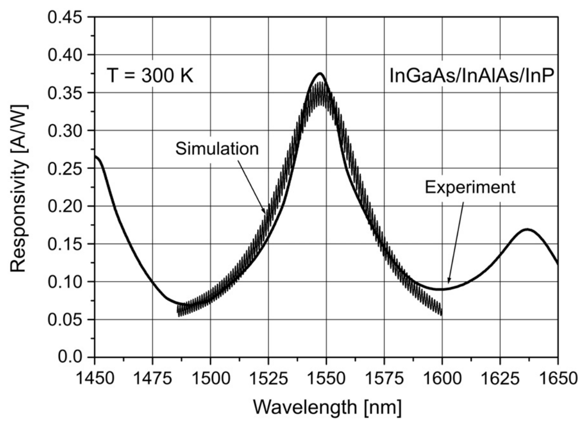

Fig. 4. The measured and simulated photoresponse of the InGaAs/InAlAs/InP RCE PD.

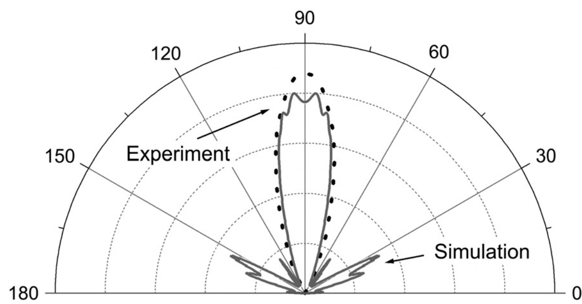

Fig. 5. Angular dependence of absorption of optimized InGaAs/InAlAs/InP RCE PD.

always been observed. They are associated with the reflectivity limit of antireflective coatings.

The resonant peak around 1548 nm was measured in good agreement with simulations. Nevertheless unexpected side peaks around 1450 and 1635 nm have also been detected in experimental data. They were not present in the simulated spectra.

The angular dependence of absorption of the InGaAs/InAlAs/InP RCE PD is shown in Fig. 5. Simulated dependence agrees well with the simulated ones. Nevertheless, higher order modes present in simulated dependence at the angles below 15° and above 150° have not been detected.

The optimized RCE PD operates efficiently only at angles of about 15° around normal incidence. This behaviour may be very useful in selected applications such as high response angle detection.

Simulations of $Hg_{1-x}Cd_xTe$ RCE photodiodes. The distributions of field intensity in the structures are presented in Figs. 6 and 7. In both cases, PDs were optimized and

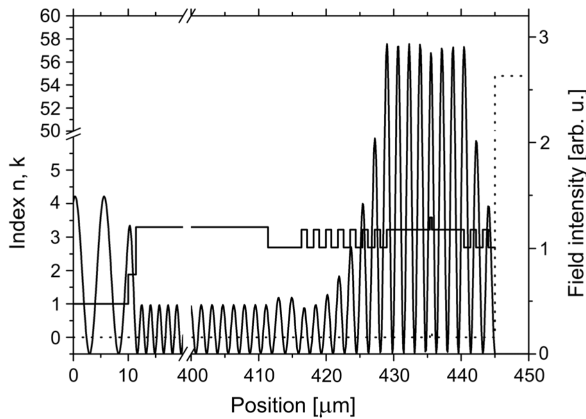

Fig. 6. Distribution of field intensity across HgCdTe/CdTe/GaAs Type 1 – DBR 7x/DBR 3x structure.

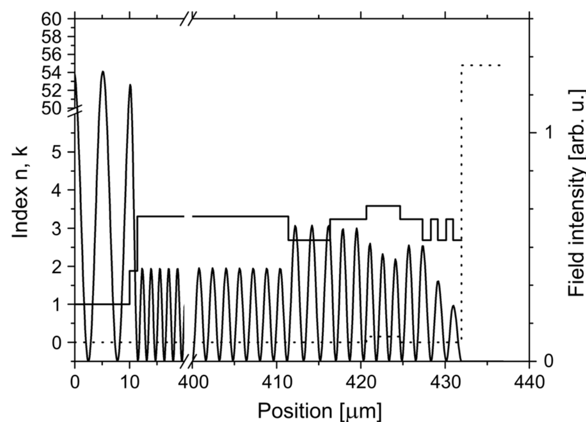

Fig. 7. Distribution of field intensity across HgCdTe/CdTe/GaAs Type 3 – DBR 0x/DBR 3x structure.

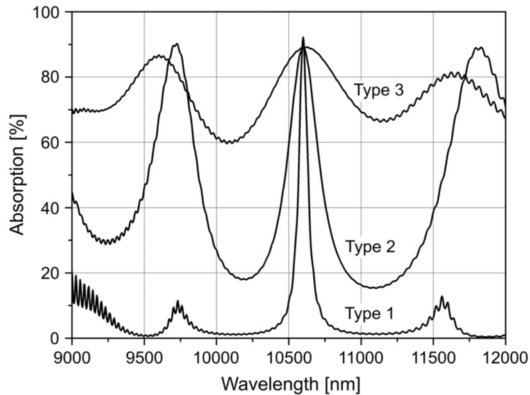

Fig. 8. The simulated absorption of different types of the HgCdTe/CdTe/GaAs RCE PD.

field intensity was centered in the middle of active layers to obtain maximum absorption. Significant changes of the layer thickness were needed to keep similar absorption level.

Spectral response for three types of HgCdTe/CdTe/GaAs structures are presented in Fig. 8. In all simulated spectra clear parasitic Fabry–Perot oscillation modes were present and for simplicity they were numerically smoothed. It is seen that in the structure equipped with 7 pairs of front HgCdTe/CdTe DBR only one, well defined, main peak is present – Type 1.

Lowering reflection of front DBR reflector up to 3 layer pairs results in the appearance of side peaks of similar heights – Type 2. Lack of the front DBR results in further modification of the spectrum – Type 3. In this case, poor quality front reflector of microcavity is formed at the air-semiconductor interface. The absorption value of the structure changes by about 30% in 9000–12000 nm spectral range. One can see that not optimized active layer thickness may result in significant lowering of detector photoresponse. Nevertheless, the thickness of all the layers and their position in the structure influence detector performance. Therefore, even in this most simple case, optical properties of complete detector structure have to be numerically simulated.

Modifications of HgCdTe/CdTe/GaAs RCE PD structures corresponds to their different angular characteristics. Simulated absorption distributions of the device for the various front mirror cases are presented in Fig. 9.

Type 1 structure with 7 period DBR operates at small angles, about ±15° near normal to detector surface. Its narrow angular characteristic is similar to the one simulated and measured for InGaAs/InAlAs/InP PDs. Two times broader angular dependence, about ±30°, is expected for Type 2 PDs. Nevertheless, really at wide angles, up to ±75°, there can operate Type 3 structures only. In this case, the devices can be monolithically integrated with microlenses formed directly onto GaAs substrate. Lenses are used to improve the performance and speed of response of photodiodes.

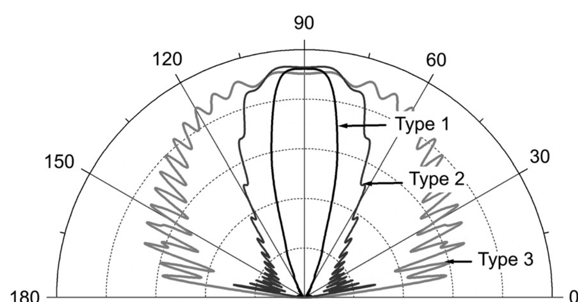

Fig. 9. Angular dependence of absorption of three types of HgCdTe/CdTe/GaAs RCE PDs.

The attempts to fabricate long wavelength $Hg_{1-x}Cd_xTe$ RCE photodiodes with $CdTe/Hg_{1-x}Cd_xTe$ Bragg reflectors were unsuccessful yet. The practical problem was large resistance of $CdTe/Hg_{1-x}Cd_xTe$ junction. Since it was larger than the detector heterostructure resistance, the device performance was severely degraded.

Our future work will be concentrated on Bragg reflectors based on heavily doped n-type $Hg_{1-x}Cd_xTe/Hg_{1-y}Cd_yTe$ pairs ($y \gg x$), where low resistance could be expected.

More successful were photovoltaic devices optimized for fast detection of quantum cascade laser radiation in which optical resonancee was based on reflection at natural device heterostructure interfaces and top metal retroreflector [8]. The device shows smoothed spectral response, peaking at selected (8, 10.3 or 10.6 μm) wavelengths. Gains by a factor of up to ≈3 were obtained when compared with non-RCE optimized devices.

5. Conclusions

We have developed resonant cavity enhanced photodiodes for fast and sensitive detection of SWIR (1.55 μm) and LWIR (≈10 μm) radiation. The devices were optimized with computer simulations and implemented using MBE and MOCVD growth.

Acknowledgements – This work was partially supported by the Ministry of Science and Higher Education under the projects No. 4 T11B 062 30 and PBZ-MiN-009/T11/2003 (experimental results on $Hg_{1-x}Cd_xTe$-based devices).

References

[1] UNLU M.S., STRITE S., *Resonant cavity enhanced photonic devices*, Journal of Applied Physics **78**(2), 1995, pp. 607–39.

[2] EL-BATAWY Y.M., DEEN M.J., *Resonant cavity enhanced photodetectors (RCE-PDs): structure, material analysis and optimization*, Proceedings of the SPIE **4999**(1), 2003, pp. 363–78.

[3] UNLU M.S., EMSLEY M.K., DOSUNMU O.I., MULLER P., LEBLEBICI Y., *High-speed Si resonant cavity enhanced photodetectors and arrays*, Journal of Vacuum Science and Technology A: Vacuum, Surfaces, and Films **22**(3), 2004, pp. 781–7.

[4] PIOTROWSKI J., GALUS W., GRUDZIEN M., *Near room-temperature IR photo-detectors*, Infrared Physics **312**(1), 1991, pp. 1–48.
[5] PIOTROWSKI J., *$Hg_{1-x}Cd_xTe$ infrared photodetectors*, [In] *Infrared Photodetectors*, SPIE, Bellingham 1995, pp. 391–494.
[6] PIOTROWSKI J., ROGALSKI A., *High-Operating-Temperature Infrared Photodetectors*, SPIE, Bellingham 2007.
[7] PIOTROWSKI A., GAWRON W., KLOS K., PAWLUCZYK J., PIOTROWSKI J., MADEJCZYK P., ROGALSKI A., *Improvements in MOCVD growth of $Hg_{1-x}Cd_xTe$ heterostructures for uncooled infrared photodetectors*, Proceedings of the SPIE **5957**, 2005, p. 108.
[8] Annual report 2006, Project No. PBZ-MiN-009/T11/2003.

Received May 14, 2007